Advances in Structural Mechanics
Volume 2, Issue 1, No. 1
Published online December 26 2022

Sanderman Publishing House

# Analysis of PV panels thermal control under different PCM properties

**H. Metwally[1], N. A. Mahmoud[1], W. Aboelsoud[1], M. Ezzat[2]**
[1]Power Mechanical Engineering, Ain Shams University, Cairo, Egypt
[2]Power Electrical Engineering, Ain Shams University, Cairo, Egypt

**Abstract.** PCM thermo-fluid properties are significant in the cooling process, so researchers studied many types of PCMs. The integration of PCM in the PV active cooling technique increases the efficiency of the cooling system. The current study focuses on the selection of the PCM, which is integrated as a heat source for the active device. PCM melting temperatures and latent heat control the amount of heat transferred from PV panels, which affect the PV panels' output. So, the selection of a suitable PCM with suitable characteristics will increase the cooling system's efficiency. The analysis of simulation results to optimize the best PCM characteristics found that the RT25 PCM presents maximum PV output power and minimizes PV panel temperature. Otherwise, the best PV panel performance is achieved when the PCM melting temperature is close to the ambient air temperature and the PCM solidification temperature is close to the water flow temperature.

**Keywords.** PCM, RT25, RT35, lauric acid, PV hybrid cooling system.

## 1. Introduction

The combination of different cooling methods aims to collect the best system performance, which is defined as a hybrid cooling system. So, rather than cooling PV panels, the addition of PCM with an active cooling source raises the cooling performance and power output. The review aims to identify the different PCM types and their effects on the PV panels' temperature. Also, try to identify the best PCM selection according melting temperature and latent heat.

PCM thermo-fluid properties are significant in the cooling process, so researchers studied many types of PCMs. Hachem et al. [1] studied experimentally the effects of using pure (white petroleum jelly) and combined PCM (white petroleum jelly, copper, and graphite) on the thermal behavior and electrical performance of a PV panel. The experimental study was provided in both cases, with and without copper and graphite molecule additions. When using Pure PCM, results showed that the PV panel's temperature decreased by 6.5 °C and the electrical efficiency increased by 3 %. Otherwise, when using PCM with additions, electrical efficiency increased by5.8%.[1]. Another PCM type (Paraffin wax 35) was studied experimentally to evaluate the PV+PCM system and the PV+PCM-T system's thermal regulation [2]. Results indicated that the PV panel temperature was reduced by 23 °C when using the PCM cooling technique, and the electrical efficiency increased by 5.18%. Another benefit is that the water was heated to 41.6 °C, requiring 1253 kJ/day more power,[2]. Hence, the addition of PCM to the PVT system indicated an electrical power output increment of 11.1% when using PCM,[3]. Novel PCM with nanoparticles was investigated in the PV panel cooling system, improving the PV panel's electrical efficiency by 25%. The selection of the appropriate PCM increased the power output by 8%–11%, [4, 5].

Aneli et al. [6] investigated the effects of two types of PCM, RT28 and RT35, on the PV panel temperature under different weather conditions. According to the findings of this study, PV+PCM units perform better than conventional PV modules, especially during the hottest months. Using RT28 and RT35 indicated an increase in the peak power of 10% and 3.5% of the energy produced, respectively. Also, when using PCM combined with a nanofluid PV cooling system, the system average thermal energy output was 42% higher than the system without PCM,[7]. Arshad et al. [8] the size of Cu nanoparticles was investigated, and it was discovered that the nanocomposite PCM with a volume fraction of 0.01 has the highest thermal storage capacity. Yadav et al. [9] investigated myristic acid PCM with carbon nanoparticles for thermal control of a 100-watt PV panel using a steady-state heat rejection rate.

Many experiments were carried out in order to find the best PCM for the passive cooling process. Kandilli and Uzel [10] investigated the effects of paraffin wax, stearic acid, and natural zeolite on the energy efficiencies of PV thermal systems. As a result of the analyses, the average energy efficiencies were estimated at 33%, 40%, 37%, and 32% for paraffin, natural zeolite, stearic acid, and the conventional PVT system, respectively. Shastry and Arunachala [11] investigated the effect of the OM-47 PCM, which enhanced thermal management by 11.1%. RT-35HC was used to investigate cooling system enhancement. They concluded that the cooling system was enhanced by 23.9% and 13.3%, respectively [12, 13].

Moreover, the CPV panel's implementation of mineral oil with graphene fillers decreased the CPV panel's temperature by 40 ºC,[14]. The experiment was conducted with different PCM materials (organic RT50, inorganic C48). The results indicated that the PCM allowed power generation up to 30 % of the maximum power values in the unglazed case. In the glazed case, the power generation was enhanced by 25% with a12% thermal improvement,[15].

A literature review illustrated that the criteria for PCM selection are different depending on the cooling application. Many studies in passive and hybrid cooling techniques choose the PCM logically and investigate its influence. The current study aims to find the best PCM selection in the hybrid cooling system. The current study tries to define the PCM characteristics by analyzing the thermal and power performance of PV panels and TEG active cooling devices under different PCM properties.

## 2. Material and Model

The Hybrid cooling model (PV+PCM+TEG+W). [16] is developed with PCM finned container technology, which consists of several modules: a PV module, a PCM module, a TEG module, and a water module.

(a) PV panels presented structured layers of glass, silicon, and Aluminum plat [17, 18].

(b) Three types of PCM with low melting temperature RT-25 [19], RT 35 [20], and lauric acid [21] are selected, as seen in Table 1.

(c) TEG products, model 1261G-7L31-04CQ, manufactured by Custom thermoelectric Co. [22] will be distributed uniformly per m2 for thermal analysis of TEG elements.

(d) The water module is 8 mm in thickness with an Aluminum cavity thickness of 1mm.

**Table 1.** PCM Thermal properties

| Properties | PCM-1 (RT-25) [19] | PCM-2 (RT-35) [20] | PCM-3 (lauric acid) [21] |
|---|---|---|---|
| Density (solid) (g/ml) | 0.88 | 0.82 | 0.94 |
| Latent heat (kJ/kg) | 230 | 157 | 187.21 |
| Melting temperature (°C) | 26 | 35 | 48.5 |
| Solidification temp. (°C) | 22 | 29 | 43.5 |
| Specific heat (kJ/kg K) | 2 | 2.1 | 2.18 |
| Thermal conductivity (W/m K) | 0.2 | 0.2 | 0.16 |
| Viscosity (kg/m s) | 0.0063 | 0.0063 | 0.0063 |
| Volume expansion (%) | 1.25 | 1.25 | 1.25 |

The study is performed for 24 hours with 12-hour daytime and 12-hour nighttime. Transient irradiation flux with maximum 900 W/m$^2$ at daytime. In addition, ambient temperature is set to 301K at daytime and 292K at nighttime.

## 3. Validation

The numerical model is validated against Huang et al. [23] experimental and numerical data for the rear and front plat temperature during the 50-, 100-, and 200-minutes simulation. Comparing the present results with Huang et al. [23] 's data shows that the maximum variance in current numerical modeling and Huang's validation is ±0.5 ºC, as seen in Figure 1.

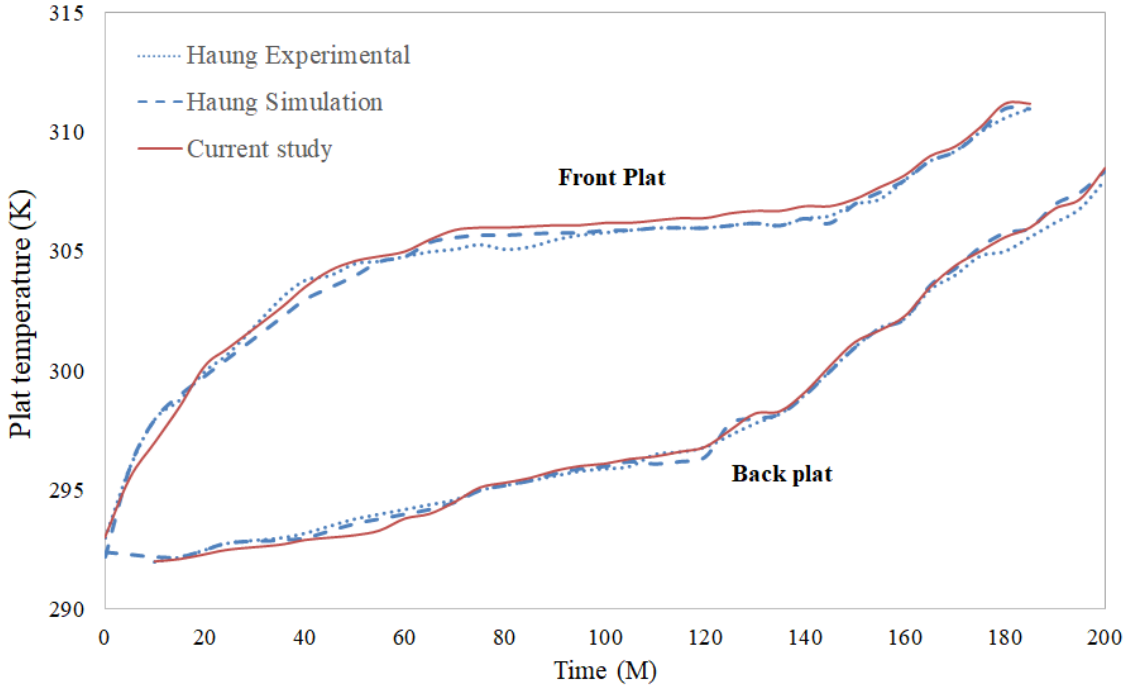


**Figure 1.** Comparison between Huang et al [23] experimental results and current study for front and back plat temperature

## 4. Mathematical Modeling

Melting or solidification process of PCM controls the heat transfer amount and PV panel cooling process [24-26].

$$\boldsymbol{\rho \frac{dH}{dt} = \nabla.(k \nabla T) - L_H \frac{\partial f}{\partial t}} \quad (1)$$

PCM enthalpy, H, described as the sum of sensible heat and the latent heat $H = C_P T + \Delta H$ [26, 27]. The Boussinesq approach considers density as a constant value except for the buoyancy term in the momentum equation [19, 29, 23].

$$\boldsymbol{(\rho - \rho_o)g \cong - \rho_o \beta (T - T_o)g} \quad (2)$$

Using Boussinesq expression, Eq. (13) can be written as follow:

$$\boldsymbol{\rho = \rho_o (1 - \beta \Delta T)} \quad (3)$$

Where $\beta$ is the thermal expansion coefficient. $\beta = -\frac{1}{\rho}(\frac{\partial \rho}{\partial T})$ . The velocity of melted PCM effects the rate of convection of heat transfer which can be measured by Local Nusselt number ($\mathrm{Nu} = \frac{h\,x}{k}$) and Stanton number ($\mathrm{St.} = \frac{h}{\rho\, Cp\, u}$) [30].

PV power generation and efficiency are stimulated by the following equation [31, 18]:

$$\boldsymbol{P_{out} = \eta A G_{pv}} \quad (4)$$

$$\boldsymbol{\eta = \eta_{ref} \left( 1 - \beta_{ref} (T_{sur} - T_{ref}) + \gamma \log_{10} (\frac{G_{pv}}{1000}) \right)} \quad (5)$$

The cooling system performance shows the effect of the cooling system and addition TEG in enhances the overall output power and define as follow:

$$\boldsymbol{COP_{Sys} = \frac{[P_{out}\,(cooled\ PV) + P_{TEG}] - P_{out}\,(individule\ PV)}{P_{out}\,(individule\ PV)}} \quad (6)$$

## 5. Results and Discussion

The simulation results identify the temperature and efficiency of the PV panel. Furthermore, the PCM heat transfer parameters Nu and St. Also, active device (TEG) thermal analysis is optimized for hybrid cooling system performance.

### 5.1. PV panel thermal management

Results compared three different PCMs with different thermal properties on the hybrid cooling system (PV+PCM/CF+TEG+W). Figure 2 depicts the variation of PV panel temperature (center of PV cell) with time as affected by irradiation flux. At noon, the PV panel temperature exceeds 322 K when applying lauric acid PCM. The use of RT35-PCM keeps the temperature of the PV panel at 315K. The minimum PV panel temperature is 307K, which is achieved by applying RT25-PCM.

Meanwhile, at night, lauric acid PCM cooled the PV panel temperature up to the ambient temperature by 2:00 AM. Otherwise, using RT35-PCM cooled the PV panel temperature up to the ambient temperature by 6:00 AM. Moreover, due to the specific heat and thermal storage of RT25-PCM, the PV panel temperature is still steady for ten hours at 5K above ambient temperature.

### 5.2. PV panel efficiency

The PV panel's efficiency increases with the decrease in panel temperature. Figure 3 depicts the effect of the PCM interface with the PV panel on heat release to the active device. The PV panel's efficiency is significantly enhanced by using RT25PCM, and this enhancement continues for eleven hours. The RT25PCM enhances the PV panel's efficiency to 15% at noon. Meanwhile, the lauric acid PCM enhances the PV panel's efficiency to 13.5%. In addition, RT35 PCM enhances the PV panel up to 14.4%. Figure 4 shows the effect of different PCM thermal storage on the system temperature contours, which indicates that the most effective PCM is RT25 at 1:00 PM and 4:00 PM.

### 5.3. PCM thermal management

PCM liquid fraction is a significant criterion in the optimization of convection heat transfer. Figure 5 presents a comparison of RT25, RT35, and lauric acid PCMs liquid fraction at 1:00 PM and 4:00 PM. Furthermore, due to the low melting temperature, the RT25 is always the highly liquid fraction, resulting in the highest fluid (melted PCM) velocity of 4.691 x 10-5 m/s and the highest fluid vorticity of 1.586 x 10-2 1/s, as shown in Figures 6 and 7, respectively. One of the most important parameters that describes convectional heat transfer is the Nusselt number (Nu). The Nusselt number can be defined as the ratio of convective to conductive heat transfer at a fluid boundary. Figure 8 shows the variation of Nu in the top of the PCM module with time from sunrise to sunset. The results show that RT25 gives the highest (Nu) by about 220 at noon. Meanwhile, the Stanton number (St) is a dimensionless group that is used to measure heat transfer.

Stanton number (St) is defined as the ratio of heat transferred into a fluid to the thermal capacity of the fluid. The results of the ST simulation at the top of the PCM module are presented in Figure 9. At noon, Lauric acid has the lowest SG, and RT25 has the highest SG by 18%.

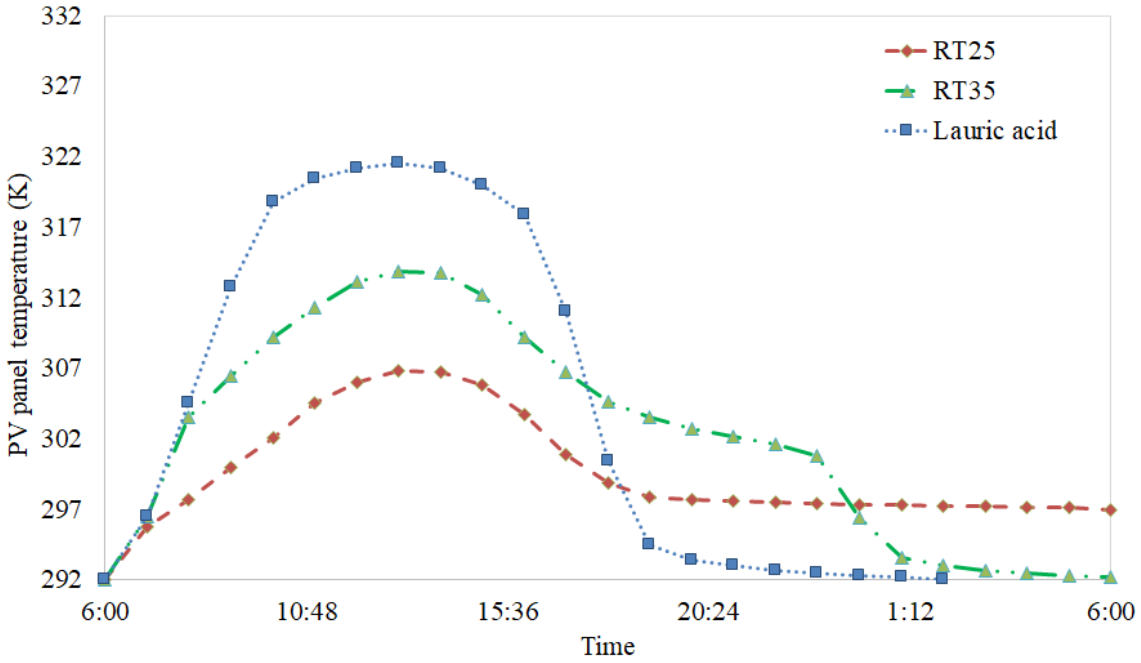


**Figure 2.** PV panel temperature analysis

### 5.4. TEG thermal management

The TEG temperature difference between the hot and cold sides of the TEG, ΔT= (TH-TC), is a significant criterion in applying a hybrid cooling system that affects the PCM selection. Figure 10 shows that using RT35 and lauric acid PCMs gives the maximum ΔTTEG by 2K at daytime. However, after sunset, the ΔTTEG reaches zero by RT35 PCM at 4:00 AM. Also, the ΔTTEG reaches zero by lauric acid PCM at 11:00 PM. Meanwhile, at nighttime applying RT25 PCM keeps ΔTTEG > 1K at nighttime until sunrise. TEG power output is a function of ΔTTEG, so applying the RT35 PCM generates more power during the day than other PCMs. Meanwhile, applying RT25 PCM generates less TEG power output than RT35 at daytime, but at night, applying RT25 conserves more power generation, as seen in Figure 11.

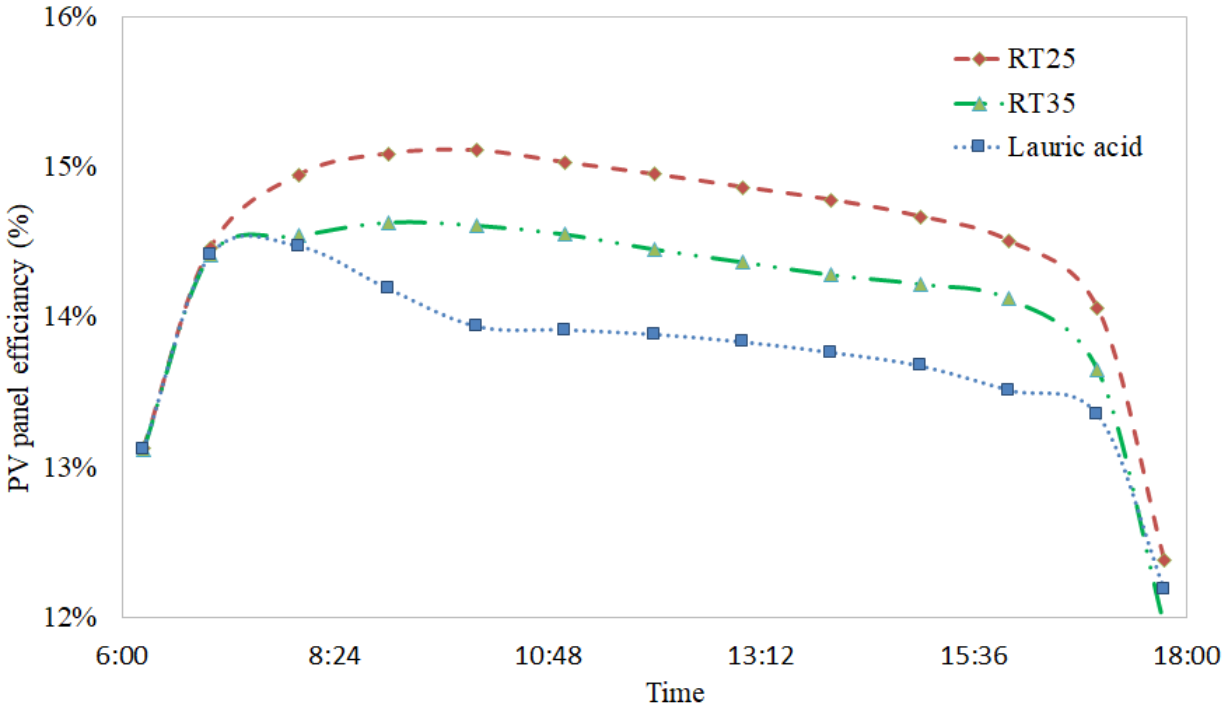


**Figure 3.** PV panels efficiency enhancement

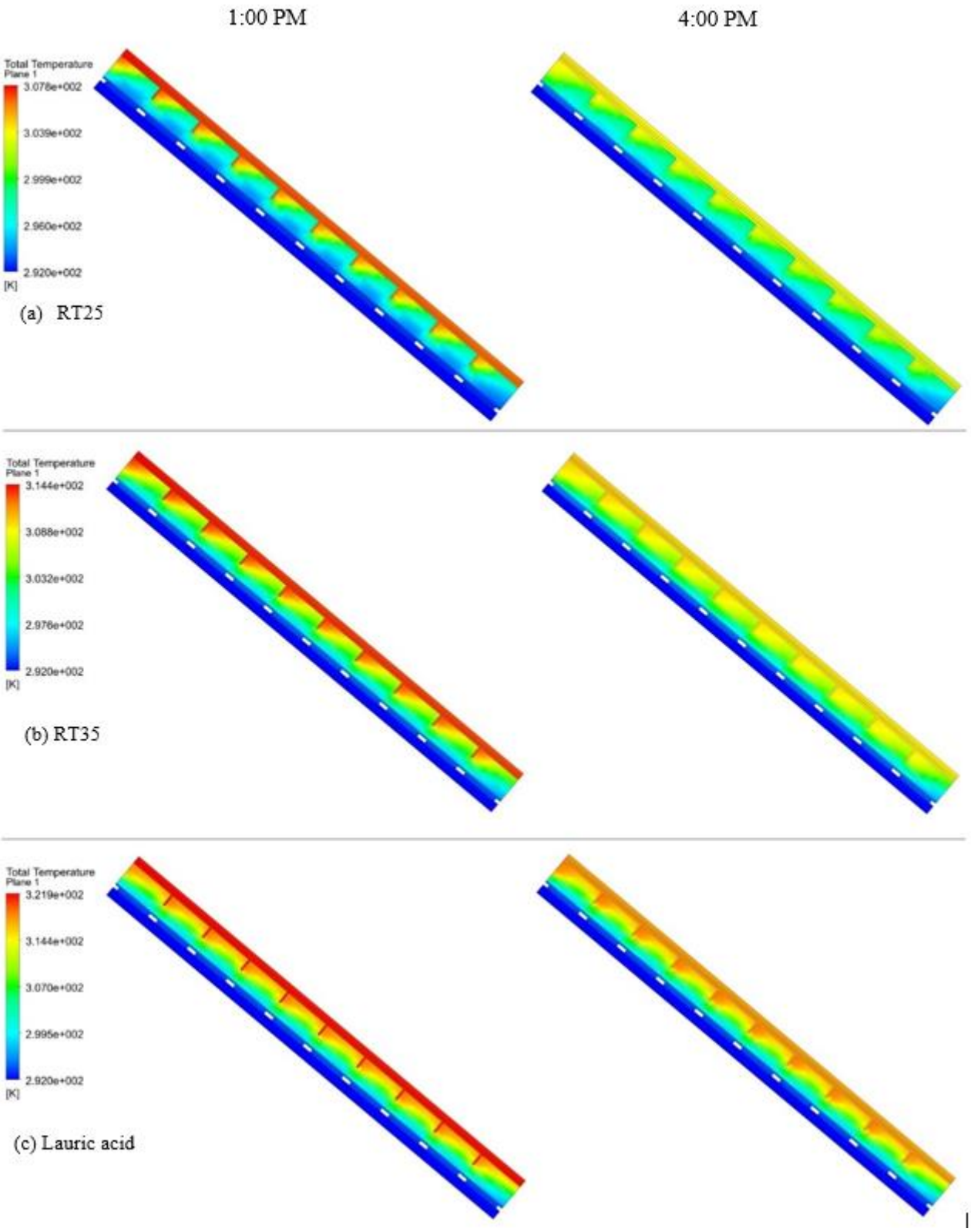


**Figure 4.** Temperature contours (a) RT25, (b) RT35, and (c) lauric acid at 1:00 PM and 4:00 PM

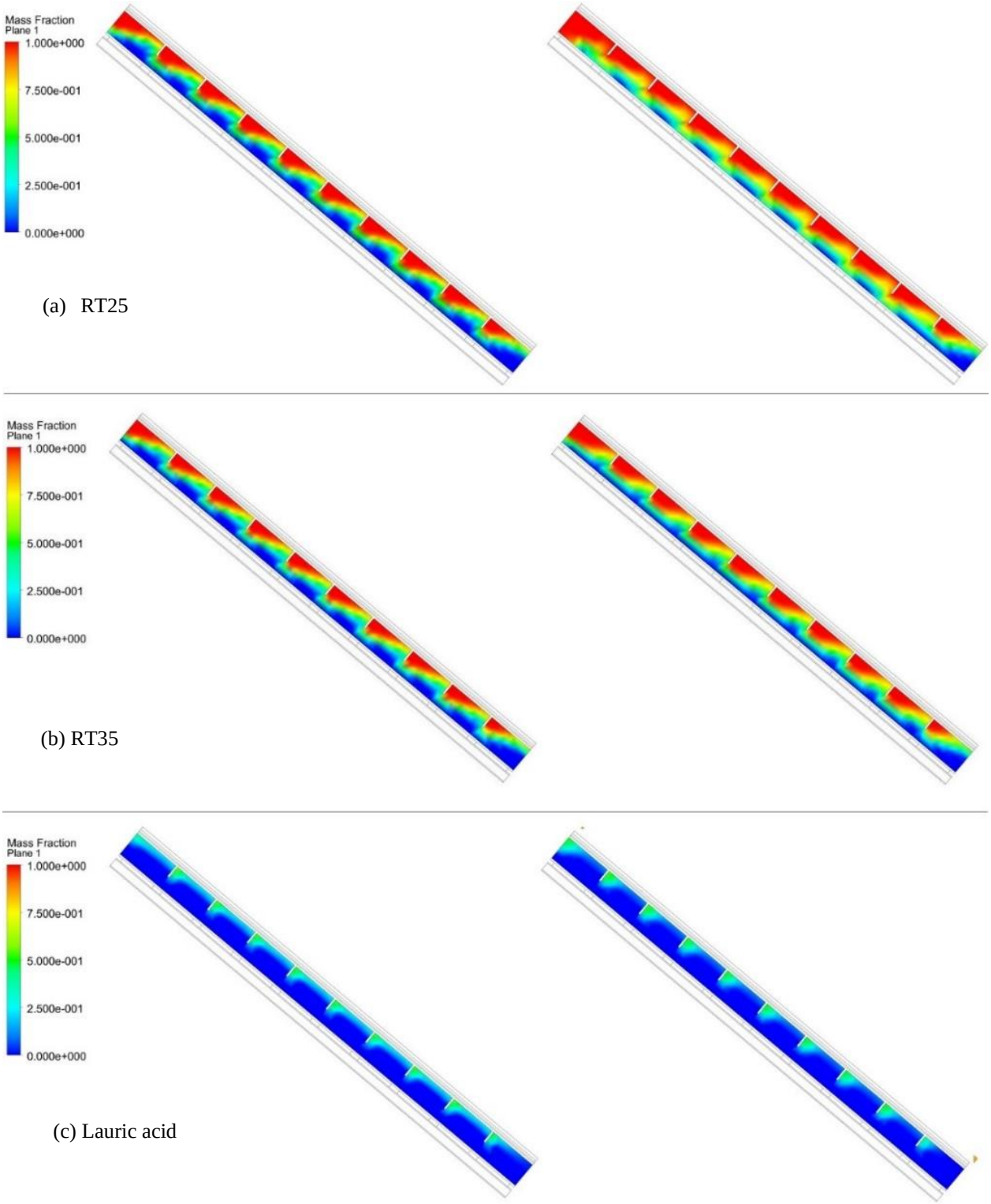


**Figure 5.** Liquid fraction (CF) of (a) RT25, (b) RT35 and (c) lauric acid at 1:00 PM and 4:00 PM

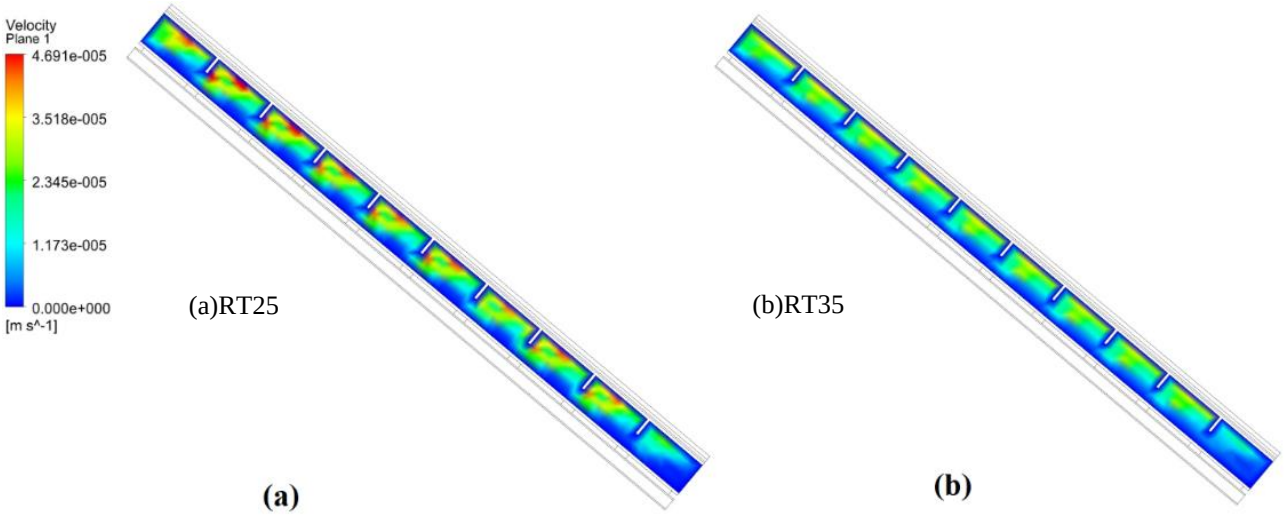


**Figure 6.** Velocity contours of (a) RT25 (b) RT35 at 1:00 PM

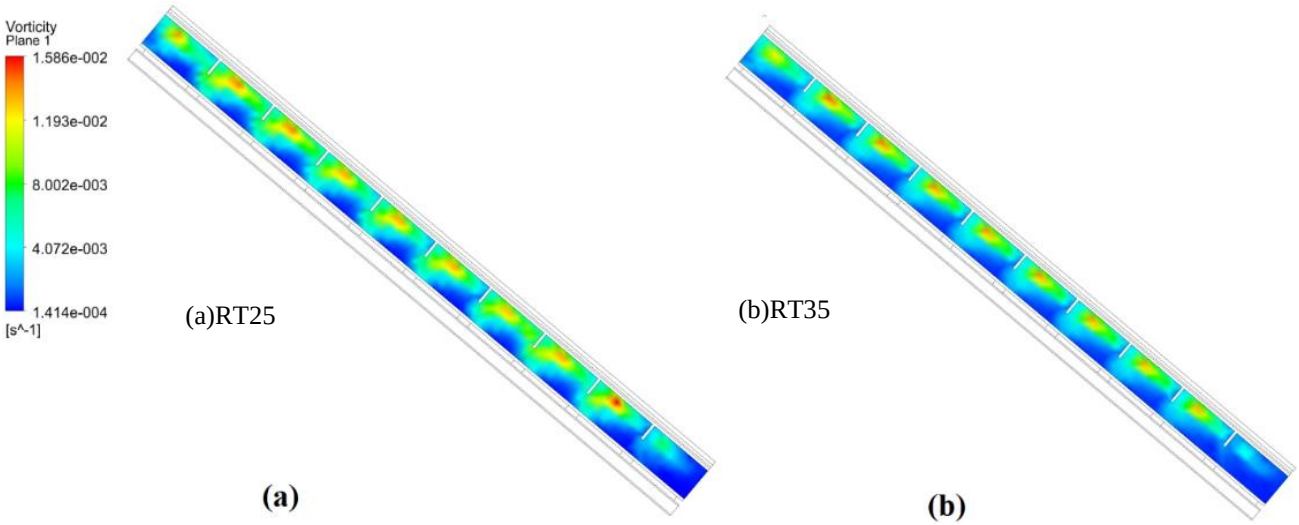


**Figure. 7.** Vorticity contours of (a) RT25 (b) RT35 at 1:00 PM

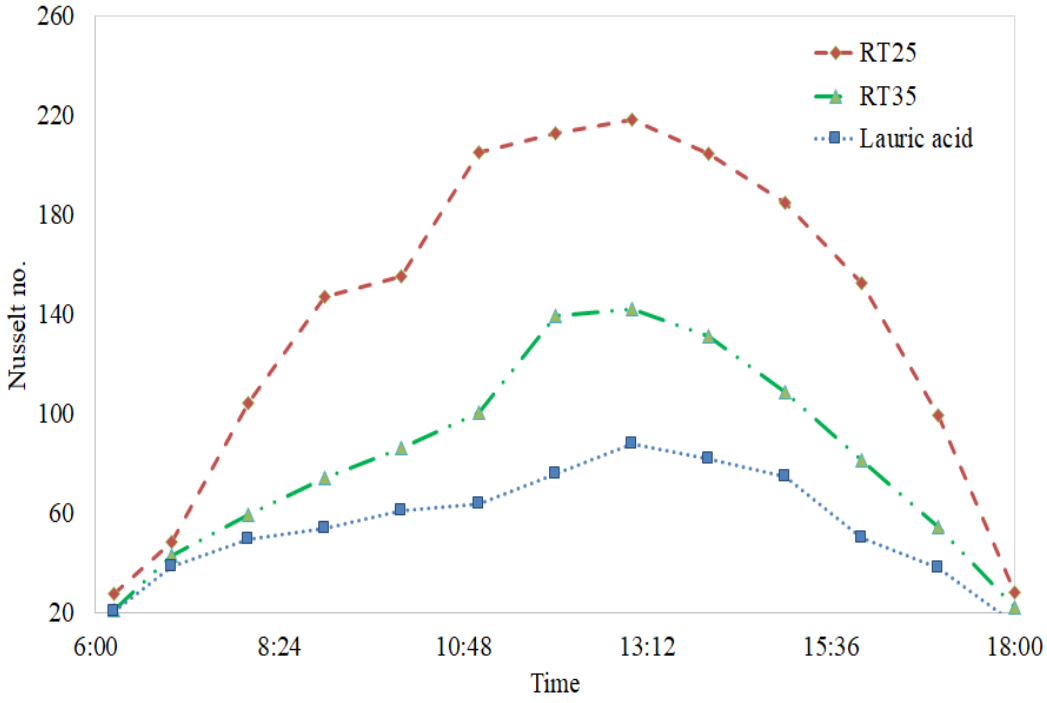


**Figure 8.** PCM Nusselt (Nu.) no. at the back plat of PV panel

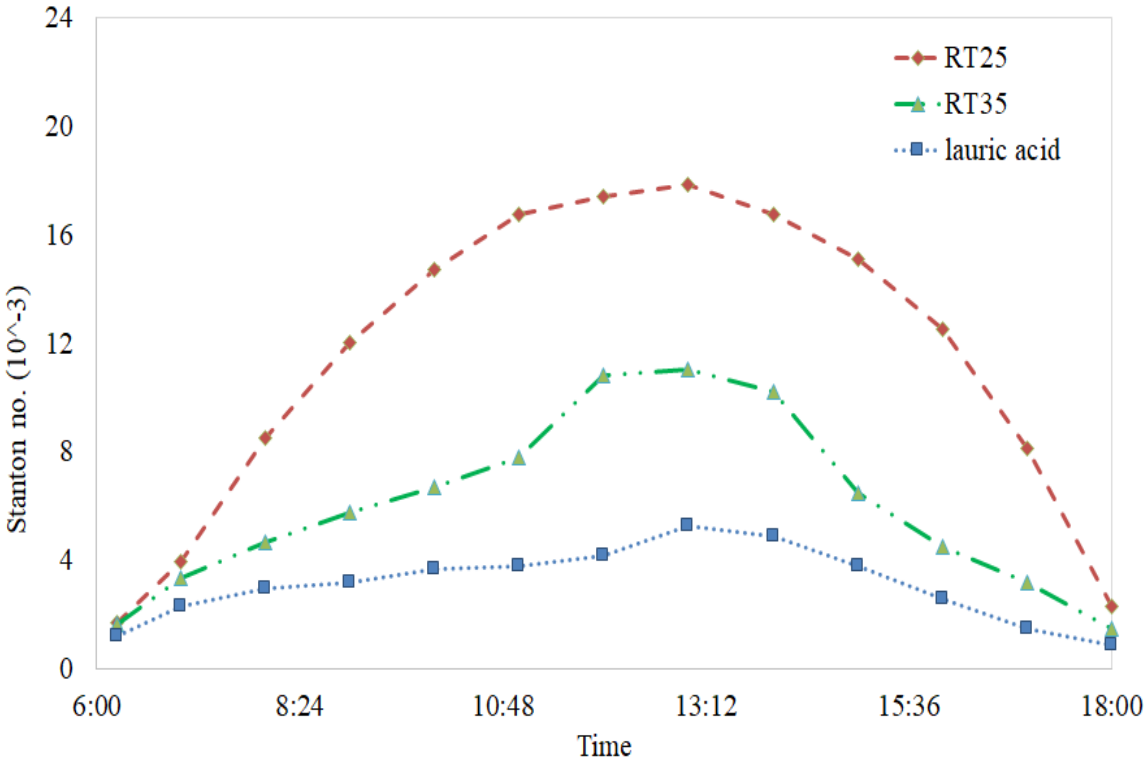


**Figure 9.** Convection heat transfer Stanton (St.) no. at the back plat of PV panel

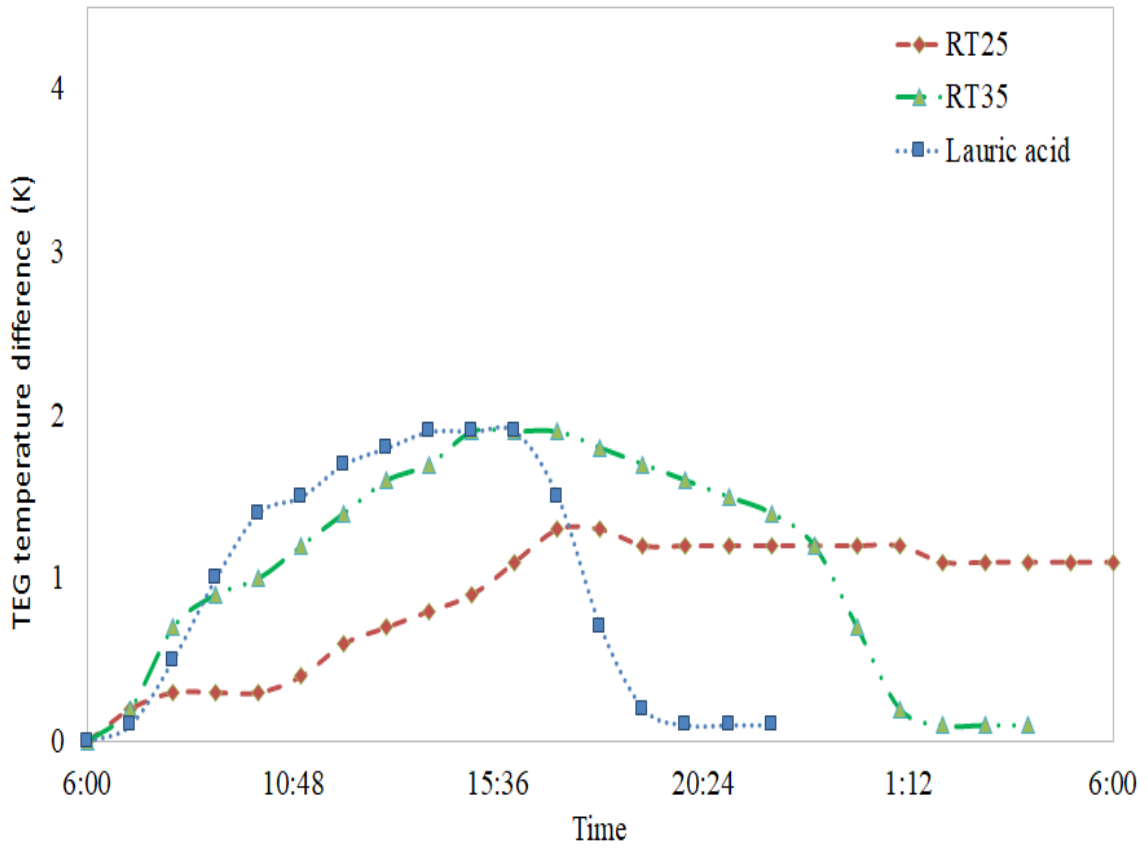


**Figure 10.** TEG temperature difference ($T_H$-$T_C$)

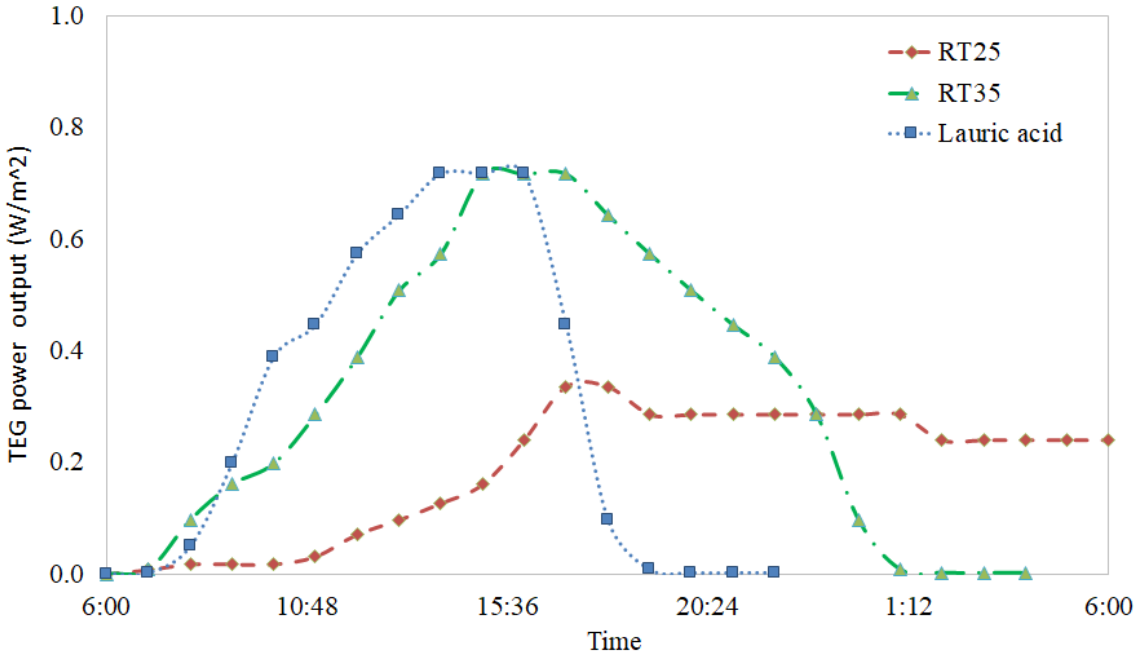


**Figure 11.** TEG electrical power output

### 5.5. System performance enhancement

Figure 12 shows that the hybrid cooling system's electrical power output is enhanced compared to the individual PV panel's electrical power output. In the case of the RT25 PCM, it is higher than other PCMs. Applying RT25, RT35, and lauric acid PCMs enhances the PV power output at noon by 22%, 16%, and 13%, respectively. Otherwise, using RT35 and lauric acid generates less power than individual PV panels by 2–4 % after 4:00 PM, when RT25 PCM provides the best performance. The hybrid cooling system performance was improved using RT25, RT35,5 and lauric acid b 20.76%,16.92% and 11.79%, respectively.

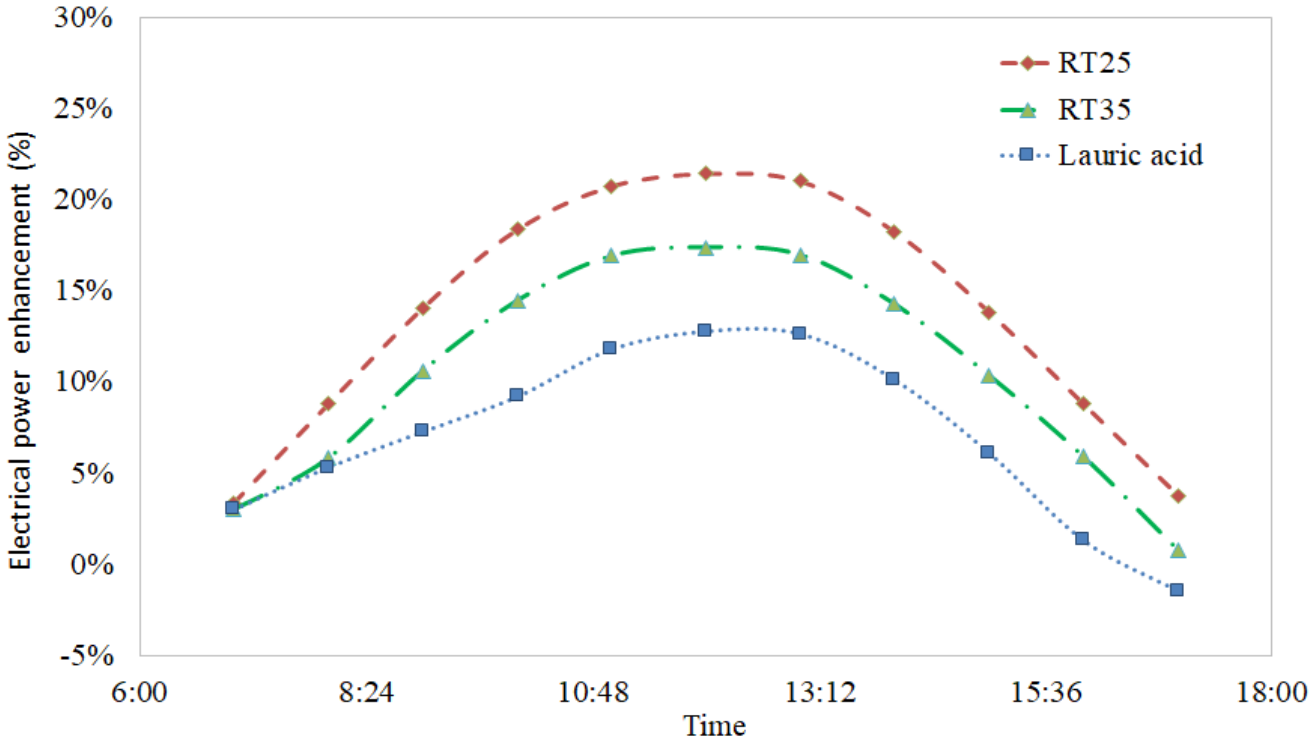


**Figure 12.** COP Hybrid cooling system performance enhancement

## 6. Conclusion

The simulation results optimized the best PCM properties in the PV panel hybrid cooling system. The hybrid cooling system depends on using PCM as a TEG heat source and water flow as a TEG heat release. Hence, with the application

of a hybrid cooling system with passive and active devices, the system performance is affected by the PCM melting temperature and latent heat.

First, a twenty-four-hour simulation shows the low melting temperature PCM (RT25) has the highest heat convection factor, the lowest PV panel temperature, and the best PV panel output power performance. Meanwhile, the TEG hot side temperature is at its maximum and generates more power than other PCM types under the same conditions due to a short time melting and a high heat transfer coefficient.

Second, a high melting temperature PCM (lauric acid) required more energy to transfer from solid to liquid and initiate natural convection. Because of, PCM's low thermal conductivity, which makes it difficult to transfer heat from the PV panel to the TEG module, natural convection is the most important heat transfer form in the application of PCM.

Finally, the PCM selection in the hybrid cooling system (PCM+TEG) must be as per two conditions. If (a) the PCM melting temperature is close to the ambient air temperature and (b) the PCM solidification temperature is close to the water flow temperature, the PCM selection provides the best performance

## NOMENCLATURE

| | | | |
|---|---|---|---|
| $A$ | Area | $Q_{in}$ | Absorbed heat by PV |
| $C_p$ | Specific heat capacity | $q_c$ | conduction heat transfer to PCM |
| $f$ | Liquid fraction of the PCM | $\Delta T$ | Temperature difference |
| $G_{pv}$ | Solar intensity | $T$ | Local temperature |
| $k$ | Thermal conductivity | $T_{Sky}$ | Sky temperature |
| $H$ | Enthalpy | $T_{glass}$ | PV panel glass surface temperature |
| $h$ | Heat convection coefficient | $T_{amb}$ | Ambient temperature |
| $L$ | Length | $a$ | Absorption coefficient |
| $L_H$ | Latent PCM heat of fusion | $\beta_{ref}$ | Coefficient of PV efficiency |
| $PCM$ | Phase change material | $r$ | Material density |
| $PV$ | Photovoltaic pane | $\eta$ | Real PV conversion efficiency |
| $q_v$ | Convection heat transfer | $\varepsilon$ | Seebeck coefficient |
| $q_{rad}$ | Radiation heat transfer | $\rho_o$ | Constant density of the flow |

## Data Availability Statements

The datasets generated during and/or analyzed during the current study are available under request from the corresponding author. Also, all data in this published article available under the web of science with DOI number as mentioned in references. Data sharing applicable to this article from the authors upon request.

## References


**[1]** F. Hachem, B. Abdulhay, M. Ramadan, H. el Hage, M. G. el Rab, and M. Khaled, "Improving the performance of photovoltaic cells using pure and combined phase change materials – Experiments and transient energy balance," Renew Energy, vol. 107, pp. 567–575, 2017, doi: 10.1016/j.renene.2017.02.032.

**[2]** Z. Li, T. Ma, J. Zhao, A. Song, and Y. Cheng, "Experimental study and performance analysis on solar photovoltaic panel integrated with phase change material," Energy, vol. 178, pp. 471–486, 2019, doi: 10.1016/j.energy.2019.04.166.

**[3]** W. Yuan et al., "Numerical simulation and experimental validation of the solar photovoltaic/thermal system with phase change material," Appl Energy, vol. 232, no. July, pp. 715–727, 2018, doi: 10.1016/j.apenergy.2018.09.096.

**[4]** L. Siahkamari, M. Rahimi, N. Azimi, and M. Banibayat, "Experimental investigation on using a novel phase change material (PCM) in micro structure photovoltaic cooling system," International Communications in Heat and Mass Transfer, vol. 100, pp. 60–66, 2019, doi: 10.1016/j.icheatmasstransfer.2018.12.020.

**[5]** C. Popp, D. Weiß, K. Tribulowski, and B. Weller, "Photovoltaic Warm Façades with Phase Change Materials in European Climates," vol. 9, no. 1, pp. 87–100, 2021.

**[6]** S. Aneli, R. Arena, A. Gagliano, and V. A. Doria, "Numerical simulations of a PV module with phase change material ( PV-PCM ) under variable weather conditions".

**[7]** M. Sardarabadi, M. Passandideh-Fard, M. J. Maghrebi, and M. Ghazikhani, "Experimental study of using both ZnO/ water nanofluid and phase change material (PCM) in photovoltaic thermal systems," Solar Energy Materials and Solar Cells, vol. 161, no. November 2016, pp. 62–69, 2017, doi: 10.1016/j.solmat.2016.11.032.

**[8]** A. Arshad, Y. Yan, M. Jabbal, H. Faraji, P. Talebizadehsardari, and M. Anser, "Numerical study of nanocomposite phase change material-based heat sink for the passive cooling of electronic components," Heat and mass transfer, 2021.

**[9]** A. Yadav, A. A. Madhavan, and V. K. Vashishtha, Numerical Modelling of Thermal Cooling in PV Panels with NEPCM. Springer Singapore, 2021. doi: 10.1007/978-981-15-9678-0.

**[10]** C. Kandilli and M. Uzel, "Exergoeconomic analysis of photovoltaic thermal systems based on phase change materials and natural zeolites for thermal management," J Therm Anal Calorim, no. 0123456789, 2021, doi: 10.1007/s10973-021-10574-z.

**[11]** D. M. C. Shastry and U. C. Arunachala, "Thermal management of photovoltaic module with metal matrix embedded PCM," J Energy Storage, vol. 28, no. January, p. 101312, 2020, doi: 10.1016/j.est.2020.101312.

**[12]** A. Hassan et al., "Thermal management and uniform temperature regulation of photovoltaic modules using hybrid phase change materials-nanofluids system," Renew Energy, vol. 145, pp. 282–293, 2020, doi: 10.1016/j.renene.2019.05.130.

**[13]** M. Qasim et al., "The effect of using hybrid phase change materials on thermal management of photovoltaic panels – An experimental study," Solar Energy, vol. 209, no. September, pp. 415–423, 2020, doi: 10.1016/j.solener.2020.09.027.

**[14]** C. Photovoltaic and S. Cells, "Non-Curing Thermal Interface Materials with Graphene Fillers for Thermal Management of Concentrated Photovoltaic Solar Cells," Journal of Carbon Research Article, vol. 6, no. 2, 2020, doi: 10.3390/c6010002.

**[15]** R. Simón-Allué, I. Guedea, R. Villén, and G. Brun, "Experimental study of Phase Change Material influence on different models of Photovoltaic-Thermal collectors," Solar Energy, vol. 190, no. July, pp. 1–9, 2019, doi: 10.1016/j.solener.2019.08.005.

**[16]** H. Metwally, N. A. Mahmoud, M. Ezzat, and W. Aboelsoud, "Numerical investigation of photovoltaic hybrid cooling system performance using the thermoelectric generator and RT25 Phase change material," J Energy Storage, vol. 42, no. July, p. 103031, 2021, doi: 10.1016/j.est.2021.103031.

**[17]** S. Boddaert, D. Caccavelli, and C. Menezo, "Hybrid PVTh Panel optimisation using a Femlab/Matlab/Simulink approach.," First International Symposium on Environment Identities and Mediterranean Area, no. 2, pp. 121–126, 2006.

**[18]** C. J. Smith, P. M. Forster, and R. Crook, "Global analysis of photovoltaic energy output enhanced by phase change material cooling," Appl Energy, vol. 126, pp. 21–28, 2014, doi: 10.1016/j.apenergy.2014.03.083.

**[19]** M. J. Huang, P. C. Eames, and B. Norton, "Phase change materials for limiting temperature rise in building integrated photovoltaics," Solar Energy, vol. 80, no. 9, pp. 1121–1130, 2006, doi: 10.1016/j.solener.2005.10.006.

**[20]** M. Babayan, A. E. Mazraeh, M. Yari, N. A. Niazi, and S. C. Saha, "Hydrogen production with a photovoltaic thermal system enhanced by phase change materials, Shiraz, Iran case study," J Clean Prod, vol. 215, pp. 1262–1278, 2019, doi: 10.1016/j.jclepro.2019.01.022.

**[21]** M. S. Hossain, A. K. Pandey, J. Selvaraj, N. A. Rahim, M. M. Islam, and V. V. Tyagi, "Two side serpentine flow based photovoltaic-thermal-phase change materials (PVT-PCM) system: Energy, exergy and economic analysis," Renew Energy, vol. 136, pp. 1320–1336, 2019, doi: 10.1016/j.renene.2018.10.097.

**[22]** TEG Specification Sheet, "TEG Specification Sheet Seebeck Thermoelectric Generator," pp. 9135–9137, 2014.

**[23]** M. J. Huang, P. C. Eames, and B. Norton, "Thermal regulation of building-integrated photovoltaics using phase change materials," Int J Heat Mass Transf, vol. 47, no. 12–13, pp. 2715–2733, 2004, doi: 10.1016/j.ijheatmasstransfer.2003.11.015.

**[24]** B. Zivkovic and I. Fujii, "Analysis of isothermal phase change of phase change material within rectangular and cylindrical containers," Solar energy, vol. 70, no. 1, pp. 51–61, 2001, doi: 10.1016/S0038-092X(00)00112-2.

**[25]** V. R. Voller and C. Prakash, "A Fixed grid numerical modelling methodology for convection diffusion mushy region phase change problems," International Jounal of Heat Mass Transfer, vol. 30, no. 8, pp. 1709–1719, 1978.

**[26]** A. D. Brent, V. R. Voller, and K. J. Reid, "Enthalpy-porosity technique for modeling convection-diffusion phase change: Application to the melting of a pure metal," Numerical Heat Transfer, vol. 13, no. 3, pp. 297–318, 1988, doi: 10.1080/10407788808913615.

**[27]** A. Hasan, S. J. McCormack, M. J. Huang, and B. Norton, "Evaluation of phase change materials for thermal regulation enhancement of building integrated photovoltaics," Solar Energy, vol. 84, no. 9, pp. 1601–1612, 2010, doi: 10.1016/j.solener.2010.06.010.

**[28]** A. C. Kheirabadi and D. Groulx, "The Effect of the Mushy-Zone Constant on Simulated Phase Change Heat Transfer," Proceedings of CHT-15 ICHMT International Symposium on Advances in Computational Heat Transfer, vol. 077, p. 22, 2015, doi: 10.1615/ichmt.2015.intsympadvcomputheattransf.460.

**[29]** "ANSYS Fluent Theory Guide," vol. 15317, no. November, pp. 724–746, 2013.

**[30]** V. Holman, "Heat transfer (tenth edition)," 1999.

**[31]** T. Ma, J. Zhao, and Z. Li, "Mathematical modelling and sensitivity analysis of solar photovoltaic panel integrated with phase change material," Appl Energy, vol. 228, no. June, pp. 1147–1158, 2018, doi: 10.1016/j.apenergy.2018.06.145.